HHS Public Access

Author manuscript

Hippocampus. Author manuscript; available in PMC 2023 March 21.

Published in final edited form as:

Hippocampus. 2023 March ; 33(3): 208–222. doi:10.1002/hipo.23476.

Postnatal Development of Hippocampal CA2 Structure and Function during Emergence of Social Recognition of Peers

Emma J. Diethorn,

Elizabeth Gould

Princeton Neuroscience Institute, Princeton University, Princeton NJ 08544

Abstract

It is now well-established that the hippocampal CA2 region plays an important role in social recognition memory in adult mice. The CA2 is also important for the earliest social memories, including those that mice have for their mothers and littermates, which manifest themselves as social preference for familiarity over novelty. The role of the CA2 in the development of social memory for recently encountered same age conspecifics, i.e., peers, has not been previously reported. Here, we used a direct social interaction test to characterize the emergence of novelty preference for peers during development and found that, at the end of the second postnatal week, pups begin to significantly prefer novel over familiar peers. Using chemogenetic inhibition at this time, we showed that CA2 activity is necessary for the emergence of novelty preference and for the ability to distinguish never encountered from recently encountered peers. In adulthood, the CA2 region is known to integrate a large number of inputs from various sources, many of which participate in social recognition memory, but previous studies have not determined whether these afferents are present by the end of the second postnatal week. To explore the development of CA2 inputs, we used immunolabeling and retrograde adenovirus circuit tracing and found that, by the end of the second postnatal week, the CA2 is innervated by many regions known to participate in social recognition, including the dentate gyrus, supramammillary nucleus of the hypothalamus, the lateral entorhinal cortex, and the median raphe nucleus. Using retroviral labeling of postnatally-generated granule cells in the dentate gyrus, we found that mossy fiber projections to the CA2 mature faster during development than those generated in adulthood. Together, our findings indicate that the CA2 is partially mature in afferent connectivity by the end of the second postnatal week, connections that likely facilitate the emergence of social recognition memory and preference for novel peers.

Keywords

Hippocampus; CA2 Region; Postnatal Development; Memory; Social Behavior; Novelty Preference

Correspondence: Elizabeth Gould, Princeton Neuroscience Institute, Princeton, New Jersey, 08544, USA. goulde@princeton.edu.

Author Contributions:

E.G. and E.J.D designed the study. E.J.D. conducted the experimental work and analyzed the data under the guidance and supervision of E.G. E.J.D. and E.G. wrote the manuscript.

Conflict of Interest:

The authors declare no competing interests

1. Introduction

Across mammalian species, social memory is an important function that forms the basis for dynamic social interactions throughout life. In humans, social memories enable healthy social interactions in families, work settings, and community living. In nonhuman primates and rodents, the ability to form and hold memories about conspecifics is crucial for determining whether social interactions are potentially threatening (Jones and Monfils, 2016; Montagrin et al., 2017), for decision-making in mating and caregiving (Ophir, 2017; Winslow et al., 1993), and for the establishment and maintenance of dominance hierarchies (Tibbetts et al., 2021). The earliest social memory is that which an infant has for its primary caregiver, usually the mother. Humans, nonhuman primates, and rodents show evidence of maternal recognition shortly after birth (Burnham, 1993; Goursaud et al., 2014; Schaal et al., 2020; Laham et al., 2021), and this recognition manifests itself as preference for the mother (Pascalis et al., 1995; Gorsaud et al., 2014; Laham et al., 2021). Humans, nonhuman primates, and rodents also show evidence of sibling recognition during early life, with a demonstrated preference for familiar social stimuli (Kostan and Snowdon, 2002; Damon et al., 2021; Clemens et al., 2020).

As development proceeds, social memory capabilities grow both quantitatively and qualitatively, with increasing ability to recognize a larger number of unrelated conspecifics and encode varied information about them (Bilkei-Gorzo et al., 2014; Okuyama, 2018). The expansion of social memory function during development is associated with an increased preference for novel social stimuli over kin during adolescence and young adulthood (Laham et al., 2021; Martinez and Howe, 2013). Although the developmental transition from preference for familiar kin to novel conspecifics has been reported in rodents (Laham et al., 2021), little is known about the emergence of social recognition for newly encountered unrelated peers, i.e., same species and age, as well as whether this type of social recognition manifests itself with novelty preference even during a time when familiarity preference for kin persists.

The hippocampal CA2 region is known to play an important role in social recognition in adulthood (Hitti and Siegelbaum, 2014; Smith et al., 2016; Meira et al, 2018). We previously reported that CA2 activation is required for mouse pups to recognize their caregiving mother during the early postnatal period, when pups prefer social familiarity, as well as after weaning, when they prefer social novelty (Laham et al., 2021). However, the role of the developing CA2 in emerging memory for novel peers remains unknown, as does whether the developing CA2 mostly functions to detect social novelty and/or to encode social memory.

In adulthood, the CA2 is a highly interconnected brain region, receiving extensive afferents from many regions both within and outside the hippocampus (Lloréns-Martín et al., 2015; Cui et al., 2014; Dudek et al., 2016). Some CA2 afferents have been shown to play critical roles in mediating social recognition memory, including those from paraventricular nucleus (PVN) (Smith et al., 2016) and the lateral entorhinal cortex (LEC) (Lopez-Rojas et al., 2022), and others appear to be more specifically involved in social novelty detection, like those from the supramammillary nucleus (SuM) (Chen et al., 2020). Although the development of the unusual molecular characteristics of the CA2 has been described

(Carstens et al., 2016; McCann et al., 2021; Laham et al., 2021), little is known about the connectivity of this brain region during the postnatal period when social preference is transitioning from familiarity to novelty. To expand our understanding of CA2 development in terms of social discrimination abilities and afferent connectivity in mice, we characterized the postnatal development of social preference for newly encountered conspecific peers and explored whether the CA2 is necessary for emerging novelty preference using chemogenetics. We also examined afferents to the CA2 during the postnatal period using labeling with retrograde adenoviruses (AAV), retrovirus axon tracing, and immunolabeling.

Here we report that, by postnatal day (P)10, most pups showed no evidence of social discrimination abilities between novel and recently encountered peers, investigating both equally. By P14, some mouse pups spent significantly more time with a novel peer, but many do not yet exhibit emerging social preference. By P21 and into adulthood, most or all mice displayed a significant preference for novel over familiar peers. We found that DREADD-induced inhibition of CA2 on P14/P15 impaired social recognition and made social preference look more similar to P10 pup behavior, suggesting that by the end of the second postnatal week, the CA2 is important not just for the social recognition memory but for the emergence of preference for social novelty. We also found that, around the time of transition of social preference from familiarity to novelty, CA2 afferents from several extrahippocampal and intrahippocampal sources are present, most showing adult-like patterns of innervation, although additional maturation appears to occur between this time and young adulthood.

2. Methods

2.1 Animals

All animal procedures were approved by Princeton University's Institutional Animal Care and Use Committee and were in accordance with the guidelines of the National Research Council's Guide for the Care and Use of Laboratory Animals. Male and female adult C57BL/6J mice were purchased from Jackson Laboratories (strain #000664) and bred in-house to produce experimental cohorts. Mice were housed in Optimice cages with bedding and nesting material, kept on a reverse light/dark cycle, and had unlimited access to food and water. Pups were weaned into same sex groups on P21. Prior to or at the time of surgery or behavior, mice either received toe tattoos (< P14) or were fitted with ear tags (≥ P14) for identification. Both male and female mice were used for all experiments.

2.2 Direct Social Interaction Test

The direct social interaction test (DSIT) was used to test social recognition on P10 (N = 10), P14 (N = 14), P21 (N = 15), and young adult (P58-P62) mice (N = 17), and to assess the impact of CA2 DREADD inhibition on emerging social memory/novelty preference on P14/P15. The DSIT was conducted in a 12" × 12" plexiglass arena (or 6" × 6" for P10) with black walls and a clear base under low light. Mice were habituated to the room for 15 minutes (min) prior to behavior. The test mouse was first habituated to the arena for 5 min 1 day prior to testing. The test consisted of two 5 min trials separated by an inter-trial interval. In trial 1 ('novel'), mice were paired with a novel age- and sex-matched

stimulus mouse from a different litter and allowed to interact freely for 5 min. After an inter-trial interval (1 hour (hr) for P10-P21 and 24 hrs for adults) during which the mice were returned to the home cage, trial 2 ('familiar') was conducted with the same test mouse and stimulus mouse pairing for 5 min. A 1 hr inter-trial interval was used for P10-P21 mice to ensure that memory of the conspecific in trial 1, if established, could be feasibly recalled in trial 2 during the same postnatal day. The test mouse and stimulus mouse were placed in the center of the arena, facing each other at a distance of 1 cm to ensure detection. The mice were placed in close proximity at the start of the test to avoid failure of the test mouse to detect the stimulus mouse. Therefore, mice with zero investigation time in either trial 1 or trial 2 were still included in all experiments, as this might represent deliberate avoidance after detection of the stimulus mouse. Both trials were recorded with a single camera directly above the apparatus, and the amount of time the test mouse spent investigating the stimulus mouse was manually scored by an experimenter blind to age, trial, and experimental condition. Investigation was defined as the test mouse orienting its nose toward and touching the stimulus mouse, with the investigation initiated by the test mouse. Pups engage in considerable huddling (Harshaw and Alberts, 2013), but this contact was excluded from the DSIT analysis, and analyzed separately (see below) because it does not involve active signs of investigation. Criteria for investigation were stringent across all experiments to ensure that the quantified behavior represents active investigation by the test mouse, as opposed to passive interaction driven by the stimulus mouse. For P10-P21 testing, a heating pad was placed beneath the arena and maintained at approximately 32°C to simulate ambient home cage temperature, as fluctuations in temperature during the early postnatal weeks have been shown to alter rodent behavior (Hofer, 1996). The arena was thoroughly cleaned with 70% ethanol between each mouse and trial.

To rule out the possibility that decreases in investigation times between the first and second trial were due to fatigue, as opposed to familiarity recognition and novelty preference, we performed two alternate versions of the DSIT on different sets of P14 pups. In the littermate version of the test, mice ($N = 6$) were first paired with a sex-matched familiar littermate in trial 1 followed by a 1 hr inter-trial interval. In trial 2, the test mouse was paired with a novel age- and sex-matched stimulus mouse, resulting in a familiar to novel test as opposed to novel to familiar. In the novel/novel version of the test, mice ($N = 9$) were first paired with a novel age- and sex-matched mouse ('novel 1') in trial 1 followed by a 1 hr inter-trial interval. In trial 2, the test mouse was paired with a new novel age- and sex-matched stimulus mouse ('novel 2'), resulting in a novel to novel test as opposed to novel to familiar.

2.3 DeepLabCut Huddling Analysis

To assess huddling behavior throughout development, and to determine whether it is altered by CA2 inhibition, time spent huddling was analyzed from the DSIT videos using DeepLabCut (Mathis et al., 2018). The DSIT was scored manually to ensure detection of brief and subtle social investigation, while DeepLabCut was used to analyze huddling because of the robust and prolonged nature of this behavior. First, videos were adjusted with color inversion, contrast, and color grading filters to remove underlying shadows within the arena. After editing, videos were exported with 1920×1080p resolution at 30 frames per second. Videos were analyzed using DeepLabCut with a Resnet-50 convolutional neural

network architecture. To begin, 500 frames were randomly selected across all behavior videos and were manually labeled for network training. On each mouse, labeled frames included nose, left ear, right ear, centroid, and tail base coordinates (Figure S1A). Following network training over 100,000 iterations, each video was manually checked to verify labeling accuracy and refine tracklets. To quantify huddling, the nose, centroid, and tail base coordinates were used to construct a model of mouse direction and interactive behavior. Huddling was defined as any frame in which the test mouse was in bodily contact with the stimulus mouse and not actively moving (determined from locomotion and nose velocity). Quantification of huddling was calculated using coordinate distances and velocities in the Spyder3 Python IDE. Distances between mice were calculated using the Cartesian distance formula.

2.4 Preparation of Viruses

The inhibitory DREADD virus (pAAV-hSyn-hM4D(Gi)-mCherry) and the control virus (pAAV-hSyn-mCherry) were generated by the University of Pennsylvania viral core and purchased through Addgene (DREADD Cat# 50475-AAV5, control Cat# 114472-AAV5). Both viruses had a titer of $\geq 7 \times 10^{12}$ genome copies per mL. For tracing CA2 circuitry, a retrograde AAV (AAV2-retro-EF1a-mCherry-WPRE-hGHpA) with a titer of 1×10^{13} genome copies per mL was generated by the Princeton Neuroscience Institute viral core. For tracing the dentate gyrus (DG) to CA2 mossy fiber projection, CAG-GFP gammaretroviruses with synaptophysin (Sim et al., 2013; Lloréns-Martín et al., 2015) and without synaptophysin (Briones et al., 2021) were generated by the Princeton Neuroscience Institute viral core. Synaptophysin (SYN), a glycoprotein localized to presynaptic vesicles, provides an indication that an axon is not only present but has the potential to make functional synaptic contact with a postsynaptic site.

2.5 Stereotaxic Surgery

For P7, P14, and adult intracranial injections, mice were anesthetized with 3% isoflurane prior to being mounted on the stereotaxic frame (Kopf 940) fitted with a nose cone adapter for neonatal (Kopf 934-B) or adult (Kopf 923-B) mice. An infrared heating pad (Kent Scientific) was placed under the animal to maintain body temperature throughout surgery. Carprofen and saline were administered in subcutaneous injections to reduce pain and maintain hydration. A scalpel was used to expose the skull and bregma was identified. To ensure evenness of the skull and accuracy of coordinates, dorsoventral (DV) measurements relative to bregma were taken from lambda, mediolateral (ML) +1.00mm from bregma, and ML −1.00mm from bregma. The ear bars and nose cone were adjusted until a DV difference of <0.10mm between lambda and bregma and between the ±1.00 ML points were confirmed. A 10μl Nanofil syringe (WPI) fitted with a 33 gauge beveled needle (WPI) was mounted into the stereotaxic frame and filled with the virus. The needle was positioned above the region of interest and burr holes were drilled at appropriate coordinates and the needle was slowly lowered down to the injection site. After injections, the burr holes were filled with bone wax (CP Medical), the scalp was sutured (Ethilon), and Vetbond tissue adhesive (Penn Veterinary Supply) was applied to further secure the sutures. Mice were then transferred to a fresh cage with a heating pad underneath to recover and returned to the home cage upon waking up. For the DREADD experiment, 50nL of DREADD or control virus was

injected into the CA2 on P7 at −1.50mm anteroposterior (AP), ±1.50mm ML, and −1.80mm DV at a rate of 20nL/min. For P14 retrograde AAV injections, 50nL of virus was injected into the CA2 at −1.80mm AP, +1.70mm ML, and −1.70mm DV at a rate of 25nL/min. For adult retrograde AAV injections, 35nL of virus was injected into the CA2 at −1.82mm AP, +2.20mm ML, and −1.69mm DV at a rate of 10nL/min. For P7 GFP-SYN retrovirus injections, 200nL of virus was injected into the dentate gyrus at −1.60mm AP, +0.90mm ML, and −1.90mm DV at a rate of 100nL/min. For P14 GFP retrovirus injections, 100nL of virus was injected into the dentate gyrus at −1.80mm AP, +1.50mm ML, and −1.80mm AP at a rate of 50nL/min. For adult GFP-SYN retrovirus injections, 1μl of virus was injected in each blade at −2.00mm AP, +1.50mm ML, −2.00mm DV (supra blade), and −2.30mm DV (infra blade) at a rate of 200nL/min. The DREADD virus and control virus were bilaterally injected and the retrograde AAV and retroviruses were unilaterally injected. To prevent the dam from rejecting surgerized pups from the nest, P7 and P14 pups were gently rolled in soiled bedding from the home cage prior to being returned to the nest.

2.6 CNO Administration

To assess the impact of CA2 silencing on social memory development, pups that received bilateral Gi DREADD or control virus injections into the CA2 on P7 underwent the direct social interaction test on P14 and P15 after administration of either saline or clozapine-N-oxide (CNO) (NIMH) dissolved in dimethyl sulfoxide and diluted in 0.9% saline. To conduct this test, mice were given an i.p. injection of CNO (0.5 mg/kg) or an equivalent volume of saline 30 min before the start of trial 1 on both P14 and P15, counterbalancing the order of injection so that all mice received both a CNO injection and a saline injection prior to the DSIT. This CNO dose was selected because pilot studies indicated that higher doses of CNO significantly diminished locomotion in both control virus and DREADD virus pups (data not shown).

2.7 Histology

Mice were deeply anesthetized with pentobarbital/phenytoin and perfused with cold 4% paraformaldehyde (20mL for ≤ P15, 40mL for > P15). Animals from the DREADD experiment received an i.p. injection of CNO (0.5 mg/kg) 30 min before perfusion to assess immediate early gene (IEG) expression in the CA2. Whole brains were extracted and post-fixed in 4% paraformaldehyde for 48 hrs, followed by cryoprotection in 0.1M PBS with 30% sucrose solution. Brains were frozen and stored at −80°C until sectioning. Brains were cut on a Leica CM3050S cryostat in 40μm-thick sections and collected into 0.1M PBS with 0.1% sodium azide.

Free-floating immunohistochemistry was performed to visualize viral infection, IEG expression, and CA2 afferent markers in the dorsal CA2. For IEG expression, four unilateral sections (±240μm from (and including) −1.80mm AP) were analyzed. For CA2 afferent markers, three unilateral sections (±240μm from (and including) −1.80mm AP (P14) or −1.82mm AP (adult)) were analyzed. All analyses were conducted on neuroanatomically-matched sections between experimental groups. Sections were first washed in 0.1M PBS for 5 min on a shaker and then transferred to a pre-blocking solution of 3% normal donkey serum in 0.1M PBS with 0.3% Triton X-100 for 1.5 hrs on a shaker. Sections

were then incubated in primary antibodies overnight. P14 (N = 12) and adult (N = 12) SuM afferents were labeled with rabbit anti-vGLUT2 (1:500µl) (Synaptic Systems, Cat# 135 403, RRID:AB_887883) and dentate gyrus afferents with rabbit anti-ZnT3 (1:500µl) (Alomone Labs, Cat# AZT-013, RRID:AB_2756813). Rat anti-mCherry (1:500µl) (ThermoFisher Scientific, Cat# M11217, RRID:AB_2536611) was used to label DREADD and control virus infection and retrograde AAV infection (1:1000µl), and rabbit anti-Zif268 (1:500µl) (Cell Signaling Technology, Cat# 4153, RRID:AB_2097038) was included in the DREADD histology to assess IEG expression in the CA2. To label GFP retrovirus infection, sections were incubated in rabbit anti-GFP (3:1000µl) (ThermoFisher Scientific, Cat# G10362, RRID:AB_2536526). All reactions included mouse anti-RGS14 (1:500µl) (Antibodies Incorporated, Cat# 75–170, RRID:AB_2179931) to visualize the CA2. After 24 hrs, sections were washed in 0.1M PBS for 5 min on a shaker and then transferred to the secondary antibody solution, which consisted of 0.3% Triton X-100 in 0.1M PBS and secondary antibodies. For afferent labeling, secondary antibodies consisted of donkey anti-rabbit 488 (1:500µl) (ThermoFisher Scientific Cat# A-21206, RRID:AB_2535792) for vGLUT2 and ZnT3, and donkey anti-mouse 568 (1:500µl) (ThermoFisher Scientific, Cat# A10037, RRID:AB_2534013) for RGS14. For DREADD virus tissue, secondary antibodies consisted of donkey anti-rat 568 (1:500µl) (Abcam, Cat# ab175475) for mCherry, donkey anti-rabbit 488 (1:500µl) for Zif268, and donkey anti-mouse 647 (1:500µl) (Millipore, Cat# AP192SA6, RRID:AB_2687879) for RGS14. For retrograde AAV tissue, secondary antibodies consisted of donkey anti-rat 568 (1:1000µl) for mCherry and donkey anti-mouse 488 (1:500µl) (ThermoFisher Scientific, Cat# A-21202, RRID:AB_141607) for RGS14. For GFP retrovirus tissue, secondary antibodies consisted of donkey anti-rabbit 488 (1:500µl) for GFP and donkey anti-mouse 568 (1:500µl) for RGS14. For GFP-Synaptophysin tissue, secondary antibodies consisted of donkey anti-rabbit 568 (3:1000µl) (ThermoFisher Scientific, Cat# A10042, RRID:AB_2534017) for GFP and donkey anti-mouse 647 (1:500µl) for RGS14. Following 1.5 hr incubation on a shaker, sections were incubated in the counterstain Hoechst 33342 (1:5000µl) for 10 min and then transferred to 0.1M PBS. Sections were then mounted on Superfrost Plus slides (Fisher Scientific) and left to dry overnight before being coverslipped with Vectashield antifade mounting media (Vector Labs) prior to imaging.

2.8 Confocal Microscopy and Image Analysis

All images were collected using a Leica SP8 confocal microscope with LASX imaging software. Images were taken with 10x or 40x objectives, and images used for quantitative analyses were collected as z-stacks with a 1µm interval between optical sections. Confocal images of vGLUT2, ZnT3, and Zif268 were analyzed using Fiji (Image J) (NIH). A rolling ball radius of 50 pixels was applied to each image prior to analysis. For vGLUT2, the RGS14+ CA2 pyramidal layer was traced with the polygon tool and the mean gray value (MGV) of vGLUT2 in each z-plane was collected and used for analysis. To account for background staining, the maximum MGV was collected from the corpus callosum, a region lacking SuM innervation, and subtracted from the maximum MGV in the CA2 for each brain section, yielding a net optical intensity. To determine the volume of the vGLUT2-labeled region, labeled areas of the CA2 pyramidal layer and stratum oriens were traced with the polygon tool. ZnT3 was analyzed in the same manner as vGLUT2, but the selected

region of interest included the RGS14+ CA2 pyramidal layer and the adjacent stratum lucidum, where dentate gyrus mossy fibers are located. Background intensity measurements were taken from the CA1, a region lacking zinc transporter, and subtracted from the maximum MGV in the CA2 for each brain section, yielding a net optical intensity. To analyze Zif268 expression in DREADD and control tissue, a minimum automatic threshold was applied, the RGS14+ pyramidal layer traced with the polygon tool, and Zif268+ cells located within this region surpassing the threshold were manually counted and divided by the volume of the RGS14+ pyramidal cell layer staining to yield cell density. For imaging of the GFP-SYN retrovirus, GFP+ mossy fiber axons were amplified with a 568 secondary antibody, detected with a red 568 laser, and pseudo-colored green. A green 488 laser was used to visualize SYN+ mossy fiber boutons, which were pseudo-colored red and were not amplified with a secondary antibody (Lloréns-Martín et al., 2015).

2.9 Statistical Analyses

All statistical analyses were conducted using GraphPad Prism 9. For the direct social interaction test, novel vs. familiar investigation time was compared across P10, P14, P21, and adult animals using a two-way ANOVA with repeated measures and Šídák's multiple comparisons. P10 mice with zero investigation time in both trials ($N = 4$) were removed from analyses. To assess social discrimination development, a one-way ANOVA with Šídák's multiple comparisons was conducted to compare the discrimination index ((novel minus familiar)/(novel plus familiar)) across ages. Total time spent huddling (trial 1 + trial 2) was analyzed using a one-way ANOVA with Šídák's multiple comparisons. The standard deviation (*SD*) of the difference score (novel minus familiar) for each age group was used to determine social preference. A difference score above one *SD* from zero was designated preference for novelty, a difference score less than one *SD* from zero indicated no social preference, and a difference score below one *SD* from zero indicated a preference for familiarity. The littermate and novel/novel versions of the direct social interaction test conducted on P14 were analyzed using paired t-tests. For the DREADD experiment, novel vs. familiar investigation times in the direct social interaction test were analyzed with a two-way ANOVA with repeated measures and Šídák's multiple comparisons between each of the four conditions: control virus + saline, control virus + CNO ($N = 9$), DREADD virus + saline, DREADD virus + CNO ($N = 9$). The discrimination indices and novel investigation times across the four conditions were analyzed using two-way ANOVAs with repeated measures and Šídák's multiple comparisons. Total locomotion (trial 1 + trial 2) between animals administered with saline and CNO were analyzed with an unpaired t-test. Total time spent huddling between saline and CNO trials in control and DREADD virus mice was analyzed with a two-way ANOVA with repeated measures and Šídák's multiple comparisons. Zif268 cell density and CA2 volume were compared between control and DREADD animals with unpaired t-tests. For CA2 afferent immunolabeling, unpaired t-tests were conducted between P14 and adult vGLUT2 and ZnT3 optical intensity and volume. All DREADD and control virus brains were validated for bilateral CA2 infection, and one DREADD animal was removed from the experiment due to lack of virus expression. Statistical analyses can be found in Table 1.

3. Results

3.1 Social recognition and preference for novel peers emerge by the end of the second postnatal week

To assess the development of social memory and preference for novel age-matched conspecifics in the postnatal period, we conducted the direct social interaction test on P10, P14, P21, and young adult C57BL/6J mice. A two-way ANOVA with repeated measures revealed a significant interaction between age and investigation time ($F_{(3, 52)} = 30.85$, $p < .0001$). At P10, there was no significant overall difference between investigation time of the novel versus the familiar stimuli ($p = .6763$) (Figure 1A). We classified the social preference of each mouse as preference for novel, preference for familiar, or no social preference and found that at P10, only a small minority of tested pups preferred the novel pup (10%), a slightly higher percentage preferred the familiar pup (20%), and the majority showed no social preference (70%). At P14, a significant difference was observed in investigation times between novel and familiar stimuli ($p = .0479$) (Figure 1A), although many pups did not show a strong social preference. At this age, no pups preferred the familiar stimulus and a greater percentage of pups preferred the novel stimulus (~43%) than at P10. At P21, there was a significant difference in investigation times between novel and familiar stimuli ($p = .0004$) (Figure 1A) and almost all pups (80%) preferred the novel stimulus with the remaining pups showing no strong social preference. By young adulthood, all mice significantly preferred novel stimuli, even with a longer inter-trial interval (24 hr compared to 1 hr) ($p < .0001$) (Figure 1A). Discrimination indices between trials increased significantly across development as the preference for novel social stimuli increased ($F_{(3, 52)} = 9.928$, $p < .0001$) (Figure 1B). The discrimination indices for P10 mice differed significantly from all other time points (P10 vs. P14, $p = .0134$; P10 vs. P21, $p = .0009$; P10 vs. Adult, $p < .0001$) while the indices from P14 mice did not differ from older animals (P14 vs. P21, $p = .9396$; P14 vs. Adult, $p = .1723$), further indicating that preference for a novel conspecific emerges around P14.

To ensure that the decrease in social investigation time between novel and familiar stimuli exhibited by P14 mice was not the result of fatigue between trials 1 and 2 of the test, we conducted two revised versions of the DSIT: the littermate test and the novel/novel test. In the littermate version of the DSIT, pups were first exposed to familiar social stimulus (sex-matched littermates) and, after a 1 hr inter-trial interval, exposed to a novel sex- and age-matched stimulus pup. In this test, investigation time significantly increased between the familiar stimulus in trial 1 to the novel stimulus in trial 2 ($t_5 = 2.672$, $p = .0442$) (Figure 1C). In the novel/novel version of the DSIT, pups were first exposed to a novel age- and sex- matched stimulus pup and, after a 1 hr inter-trial interval, exposed to a new novel age- and sex- matched stimulus pup. In this task, investigation times did not significantly differ between trials ($t_8 = 0.9988$, $p = .3471$) (Figure 1D), indicating sustained interest for novel social stimuli across consecutive presentations. These additional findings confirm that reduced investigation times at P14 in trial 2 of the standard DSIT were not due to the order of testing, but rather to an emerging novelty preference.

To assess whether time spent huddling, a non-investigative social behavior, also changes with age, we used DeepLabCut to track and quantify huddling from the DSIT videos (Figure S1A). In this analysis, there was a significant effect of age on total time spent huddling (trial 1 + trial 2) ($F_{(3, 52)} = 9.647$, $p < .0001$) (Figure S1B). No differences in time spent huddling were found between P10 and P14, as mouse pups still live in the nest, huddling with their littermates ($p = .4056$). By P21, the day of weaning, time spent huddling drops significantly as mouse pups are able to maintain body temperature outside of the nest (P10 vs. P21, $p = .0311$; P14 vs. P21, $p < .0001$). Adult mice spent the lowest time huddling of all ages (Terranova & Laviola, 1995), doing so only in short bursts during social interaction trials, though huddling time did not differ significantly from P21 (P10 vs. Adult, $p < .0001$; P14 vs. Adult, $p < .0001$; P21 vs. Adult, $p = .0966$).

3.2 Chemogenetic inhibition of CA2 impairs social memory in mouse pups

We found that, by P14, mouse pups significantly decrease investigation for familiar compared to novel social stimuli. To determine whether the CA2 is necessary for this behavior, as it is in adult mice, we injected an inhibitory DREADD virus (pAAV-hSyn-hM4D(Gi)-mCherry) ($N = 9$) (Figure 2B and 2D) or a control virus (pAAV-hSyn-mCherry) ($N = 9$) (Figure 2C) into the CA2 bilaterally on P7 and administered CNO (0.5 mg/kg) or saline (i.p.) 30 min prior to the start of the direct social interaction test on P14/P15. Each mouse received a CNO or saline injection on P14 prior to behavior, and a CNO or saline injection on P15 prior to behavior. CNO and saline trials were counterbalanced and separated by 24 hrs to account for lingering effects of CNO. After testing on P15, pups were perfused to confirm viral infection (Figure 2A). While viral infection was most intensely localized to CA2, some sparse staining was observed in dorsal CA1, CA3, and DG (Figure S2A), and was observed in both RGS14+ pyramidal cells and RGS14− putative interneurons (Figure S2B–E). To confirm CA2 inhibition, CNO-treated control virus and DREADD virus pups were examined for Zif268 labeling in the CA2 as a proxy for neuronal activation (Figure 2E and 2F). Zif268 expression was observed in virus-infected RGS14+ pyramidal cells as well as in RGS14− putative interneurons (Figure S3). Some DREADD-infected pyramidal cells and putative interneurons lacked Zif268 expression, presumably due to CNO administration (Figure S3B and D). DREADD virus mice administered CNO had significantly lower Zif268 cell density in the CA2 than control virus mice administered CNO ($t_{16} = 3.115$, $p = .0067$) (Figure 2J). This analysis was conducted on neuroanatomically matched sections and the analyzed volume of the CA2 was not different between conditions (unpaired t-test: $t_{16} = 1.791$, $p = .0922$) (data not shown).

A two-way ANOVA with repeated measures revealed a significant interaction between trial and condition in the direct social interaction test ($F_{(3, 32)} = 4.291$, $p = .0118$) (Figure 2G). We found significant decreases in investigation times between novel and familiar stimuli in control conditions (pups infected with control virus followed by saline ($p = .0428$) or CNO ($p = .0127$), as well as those infected with DREADD virus followed by saline ($p = .0016$)), while pups infected with DREADD virus followed by CNO eliminated this difference ($p = .9186$). The majority of mice in the DREADD virus plus CNO condition showed no social preference. Analysis of the discrimination index for each condition in two-way ANOVA with repeated measures revealed a significant interaction between discrimination index and

condition ($F_{(1, 16)}$ = 6.315, p = .0231) (Figure 2H). While control mice exhibited no change in discrimination index between saline and CNO trials (p = .8533), the discrimination index of DREADD mice was significantly decreased in the CNO trials compared to the saline trials (p = .0154). We assessed differences in time spent investigating the novel conspecific in trial 1 using a two-way ANOVA with repeated measures and found no significant interaction between novel investigation time and condition, indicating that CNO did not alter sociability across conditions ($F_{(1, 16)}$ = 0.0617, p = .8069) (Figure 2I). With an unpaired t-test, we found that total locomotion time (trial 1 + trial 2) between animals administered saline or CNO were not significantly different, confirming that CNO alone had no effect on general activity (t_{34} = 0.0844, p = .9332; saline: 43.2 ± 6.75 sec., CNO: 42.43 ± 6.12 sec.) (data not shown). Analysis of huddling behavior using DeepLabCut yielded no significant interaction between virus and treatment in the total time spent huddling ($F_{(1, 16)}$ = 0.04486, p = .8349) (Figure S1C), indicating that administration of CNO had no impact on non-investigative social behavior.

3.3 The CA2 receives similar projections at P14 as in adulthood

To determine whether known afferents to the adult CA2 are present at P14, we injected a retrograde AAV containing mCherry into the CA2 at P14 (Figure 3A) and young adulthood (Figure 3B) and perfused mice 2 weeks post-injection (WPI). Retrograde AAV is picked up by axon terminals at the injection site and transported back to the cell bodies of origin, providing evidence of afferent projections to the CA2. Using this method, we found that a number of known projections in the adult CA2 are present by P14, including projections from the dentate gyrus (DG), supramammillary nucleus (SuM), lateral entorhinal cortex (LEC), and the median raphe nucleus (mRN) (Figure 3C–F). The same projections were identified in adulthood using the same method (Figure 3G–J). These findings suggest that around the time when preference for social novelty emerges, the CA2 is likely receiving input from a number of sources that may be critical for this function. mCherry+ backfilled cells were not found in other regions known to project to the CA2, including the ventral tegmental area (Martig and Mizumori, 2011), locus coeruleus (Wagatsuma et al., 2017), the paraventricular nucleus (Cui et al., 2020), and the medial and lateral septal nuclei (Cui et al., 2020), although this lack of labeling was observed in both P14 and adult brains, suggesting that it was not a developmental phenomenon and may be because retrograde transport of the virus to these regions requires more time.

To better characterize the postnatal development of the dentate gyrus to the CA2 projection, we utilized both a GFP retrovirus and a GFP-Synaptophysin (GFP-SYN) retrovirus to visualize mossy fiber axons and their synapses with CA2 pyramidal cells. Retroviruses were injected into the DG in P7, P14, and adult mice. The retrovirus infects any cells currently dividing at the time of injection, which is a frequent occurrence in the DG, a major site of postnatal neurogenesis. P7 mice were perfused at 2 WPI, P14 mice at 4 WPI, and adult mice at 6 WPI to allow time for granule cell (GC) mossy fibers to extend to the CA2. We found GFP+ mossy fiber axons innervating RGS14+ CA2 pyramidal cell dendrites in the stratum lucidum and cell bodies in the stratum pyramidale at all ages examined, indicating that granule cells born as early as 7 days after birth and onward project to the CA2 (Figure 4A–C). We also noted, as expected due to the longer post-injection time,

increased dendritic tree complexity and arborization of granule cells in adult-injected mice compared to P14-injected mice (Figure 4F and 4G) (van Praag et al., 2002). In adult mice, abGC mossy fiber axons first appear near the CA2 2 weeks after neuronal birth, but do not make SYN+ contact until 3 weeks at the earliest (Lloréns-Martín et al., 2015). Using the GFP-SYN retrovirus, we found colabeled GFP+ mossy fiber axons and SYN+ boutons in the stratum lucidum emanating from P7-born granule cells 2 weeks after cell division (Figure 4D i–iii), suggesting that the process of synaptic connectivity between the DG and CA2 may occur at an accelerated rate during development than in young adulthood. We observed SYN+ varicose mossy fibers in the stratum lucidum of adult animals perfused 6 WPI (Figure 4E i-iii), as previously reported (Lloréns-Martín et al., 2015).

3.4 Markers of SuM and DG afferents are present in the CA2 by P14 and increase in intensity by adulthood

Because viral tracing studies are difficult to analyze quantitatively due to the fact that virus injections, uptake, and expression may differ across ages, we sought additional data about two afferent populations with known markers: the supramammillary nucleus, whose CA2 afferents are important for social novelty detection (Chen et al., 2020), and whose glutamatergic afferents can be labeled with vGLUT2 (Figure 5A and 5B), as well as the dentate gyrus, which has been linked to social memory (Leung et al., 2018; Cope et al., 2020) and whose mossy fiber afferents can be labeled with ZnT3 (Figure 5E and 5F). We found robust labeling of both markers in the CA2 at P14 and, in both cases, the intensity of these labels increased by young adulthood (vGLUT2: $t_{22} = 5.142$, $p < .0001$; ZnT3: $t_{22} = 11.71$, $p < .0001$) (Figures 5C and 5G). The volume of the vGLUT2-labeled region increased with age ($t_{22} = 2.087$, $p = .0487$) (Figure 5D) suggesting that the size of the supramammillary projection increased with time, while the volume of the ZnT3-labeled region did not ($t_{22} = 0.4330$, $p = .6692$) (Figure 5H), suggesting that this projection may be adult-like in size by P14. The presence of substantial labeling in the CA2 at P14 provides additional evidence that projections from the supramammillary nucleus and dentate gyrus are present and may be contributing to emerging social recognition and social novelty preference. Likewise, the further increase in labeling intensity of both markers between P14 and young adulthood may indicate the growth of physiological properties underlying social recognition capabilities.

4. Discussion

These findings provide evidence of postnatal development of social recognition function for peers in mouse pups. We found that at P10, most pups do not distinguish between novel and familiar same-age, same-sex social stimuli and those that do have mixed preferences, with some investigating familiar more than novel as well as vice versa. By P14, familiarity preference for peers was no longer observed, with many more pups preferring the novel social stimulus. Novelty preference increased further by weaning, and became quite robust in young adulthood. Using chemogenetic inhibition, we found that the hippocampal CA2 is necessary for developmental social recognition of peers and for emerging novelty preference on P14/P15, with DREADD + CNO animals exhibiting diminished preference for a novel conspecific and mostly showing no preference for either novel or familiar social stimuli.

Coincident with the developmental emergence of social memory, we found that several afferent populations, which have been shown to be important for social recognition in adulthood, are present in the CA2 by P14, including those from the supramammillary nucleus of the hypothalamus and the granule cells of the dentate gyrus. Although present at this early time point, both projections seem to undergo further growth between the end of the second postnatal week and into adulthood. Taken together, these results suggest that the ability to recognize peers and respond with decreased investigation of the familiar stimulus occurs around a developmental time when the basic structure of the hippocampal circuit supporting adult social recognition and preference for novelty is in place.

Our previous work showed that mouse pups exhibit a familiarity preference toward their caregiving mothers as early as P3, behavior that is mostly driven by experience since even genetically unrelated pups display this preference for their caregiving mothers (Laham et al., 2021). Preference for the caregiving mother over a novel mother begins to reverse toward the time of weaning, as juvenile and adult mice show preference for novel social stimuli in the caregiver test (Laham et al., 2021). Familiarity preference for kin during the early postnatal period seems adaptive since prior to weaning, preference for the familiar mother and littermates increases the likelihood that pups will remain in the nest where food, warmth, and protection are provided. After weaning, when offspring are more capable of finding their own food and shelter, the survival benefits of familiarity preference are likely outweighed by any potential benefits of social novelty preference.

Our data indicate that, at P10, mouse pups show no preference for peers based on novelty or familiarity, despite demonstrating a preference for kin (Laham et al., 2021). It seems likely that kin preference is due to long-term social exposure in the home cage, enabling a robust memory to form that manifests as a preference for familiarity at a time when doing so is adaptive. In our experiment, one brief interaction with a novel peer seems to be insufficient for a memory to form at P10, preventing pups from displaying any peer preference at this time. The ability to discriminate between novel and recently encountered peers emerges toward the end of the second postnatal week, and we found that the majority of pups tested at this time investigated a novel peer more than a familiar littermate. In the wild, weaning is a protracted process that begins around the end of the second postnatal week when pups' eyes open and they become more mobile (Bailoo et al., 2020). The coincidence of this time with increased ability to form memories of newly encountered peers may be additionally beneficial for ramping up a social memory function that is required for navigating social hierarchies and ultimately for decision-making in reproductive behavior.

Numerous studies have shown that the CA2 region plays a critical role in social recognition memory in adult mice (Hitti and Siegelbaum, 2014; Smith et al., 2016; Meira et al., 2018; Laham et al., 2021), and that this region responds to familiar social stimuli with reduced activity of pyramidal neurons (Oliva et al., 2020; Laham et al., 2021). Our previous study using chemogenetic inactivation in mouse pups at P10 showed that the CA2 is involved in memory for mothers even when the behavioral manifestation of social memory is preference for familiarity (Laham et al., 2021). Taken together with the current findings that CA2 inhibition eliminates a novelty preference observed in the formation of new memories about recently encountered peers suggests that this brain region is important for social

recognition memories regardless of whether the response is higher investigation of novel or familiar stimuli. The heterogeneity of responses to social stimuli that are present at the end of the second postnatal week may be due to individual differences in circuit-level development related to the CA2. Thus, although our neuroanatomical data suggest that afferents to the P14 CA2 seem qualitatively similar to those in the adult CA2, with evidence from retrograde viral tracing of inputs from the supramammillary nucleus, dentate gyrus, entorhinal cortex, and raphe nucleus comparable to those observed in adulthood, it should be noted that the use of retrograde tracers is not conducive to rigorous quantitative analysis given potential variation in the viral infectivity and expression across brains, especially at different ages. It is therefore not possible to determine from our data whether the strength of these connections changes over time. However, immunolabeling studies of specific afferent markers allow for quantitative analyses that show further development occurs between this time and young adulthood, at least for inputs from the supramammillary nucleus and the dentate gyrus. Since supramammillary inputs to the CA2 are important for social novelty recognition (Chen et al., 2020) and are among the first afferents observed in the CA2 during embryonic development of primates (Berger et al., 2001), the early postnatal development of this circuit may be a key determinant in the shift to novelty preference in response to peers. Future studies linking brain changes to individual differences in social recognition during the transition to novelty preference may help to answer this question, as would specific manipulations of supramammillary inputs to the CA2 during development.

The dentate gyrus has also been linked to social memory in adulthood (Cope et al., 2020; Leung et al., 2018) and is known to project to the CA2 region (Kohara et al., 2014; Lloréns-Martín et al., 2015), raising the possibility that this projection plays an important role in social recognition. To characterize the development of dentate gyrus afferents to the CA2, we used retroviruses to label postnatally-generated granule cells and trace their nascent axons to the CA2. We found that granule cells born during the first and second postnatal weeks of life extend axons into the CA2, and some of our evidence suggests a slightly accelerated rate of development during the early postnatal period, with granule cells forming putative synaptic connections with the CA2 more rapidly than in adulthood. Lloréns-Martín and colleagues (2015) previously reported that adult-born granule cell mossy fibers form synaptophysin+ connections with CA2 pyramidal cell apical dendrites in the stratum lucidum as early as three weeks after cell proliferation and viral infection, and our findings indicate that this process occurs more rapidly during the early postnatal period, with synaptophysin+ connections forming just two weeks after neuronal birth, by P21. It is important to note that mouse granule cell genesis starts during embryonic life (Stanfield and Cowan, 1979; Angevine, 1965) and these neurons are likely to have axons in the developing CA2 as well. Although we do not have direct evidence for this, the presence of ZnT3+ fibers in the CA2 at P14 as well as substantial retrograde AAV-labeled granule cells after P14 injection strongly suggest this is the case. While some DREADD virus brains exhibited sparse viral labeling in the DG and mossy fiber pathway (Figure S2A), the role of developmentally-generated granule cells in emerging social memory has not yet been explored, and the effect that inhibiting these cells would have during the early postnatal period is unknown.

It should also be noted that a number of known projections to the adult CA2 were not observed in our studies with the retrograde AAV following injections at P14 and in adulthood. Unexpectedly, given previously reported studies in the adult brain (Martig and Mizumori, 2011; Wagatsuma et al., 2017; Cui et al., 2020), mCherry+ cells were not observed in the ventral tegmental area, locus coeruleus, nor in the medial and lateral septal nuclei. The reasons for these discrepancies may be related to differences in the tracer used, the size of the injection or infection, as well as in developmental expression of promoters. It is also possible that adequate retrograde labeling of these regions requires a longer post-infection time than that used in the current study, i.e., two weeks.

An unusual feature of the CA2 is its dense concentration of perineuronal nets (PNNs) surrounding pyramidal cells and parvalbumin+ (PV) inhibitory interneurons (Dudek et al., 2016; Cope et al., 2021). This unusual extracellular composition raises the possibility that the earliest social recognition of peers observed in our study may be dependent on the development of properties intrinsic to the CA2, as opposed to or in addition to innervation from other regions. Along these lines, it has been reported that long-term depression (LTD) of PV+ interneuron inhibition of CA2 pyramidal cells is absent in early postnatal development, and its appearance along with that of PNNs has been reported to contribute to emerging social memory (Dominquez et al., 2019). However, this form of plasticity does not occur until well after weaning, making it unlikely that LTD at PV+ interneuron synapses plays a crucial role in the emergence of social preference for novelty around P14. Inhibitory interneuron activity may still contribute to emerging novelty preference in the second postnatal week, since DREADD virus infection was observed in RGS14+ pyramidal cells as well as in RGS14− putative interneurons in the CA2, whose activity would also be inhibited in the presence of CNO. Further chemogenetic inhibition studies targeting specific cell populations during early postnatal development of the CA2 may elucidate the role of inhibitory interneurons vs. pyramidal cells in emerging novelty preference. We observed sparse viral labeling in CA3 and, since this region innervates the CA2 and contributes to social discrimination abilities (Chiang et al., 2018; Boehringer et al., 2017), chemogenetic modulation of CA3 cells may also have contributed to the observed DREADD + CNO effect by altering additional hippocampal regions key to social behavior. Viral infection was also observed in dorsal CA1 but did not extend into ventral CA1 (Figure S2Av), the latter of which receives projections from CA2 and is involved in social memory (Meira et al., 2018). The ventral CA1 in turn projects to the prefrontal cortex which is a region that, along with its connections to reward circuitry, is known to function in social memory. Future studies examining downstream targets of the CA2-ventral CA1 circuit in the context of development would be useful for understanding the broader circuitry supporting the emergence of this function.

Impairments in social recognition memory are features of some neurodevelopmental disorders, including Autism Spectrum Disorder, Phelan-McDermid syndrome, and Fragile X syndrome (Guillory et al., 2020; Williams et al., 2012; Holsen et al., 2018). Since social memory is critical for healthy function in home, school, and work settings, both during development and in adulthood, understanding the developmental trajectory of social memory and how the circuitry required for this development forms in the healthy brain likely has translational relevance. The current findings extend our understanding of the development of

social recognition of peers in control mice and verify the critical involvement of the CA2 in this function, as well as begin to describe the formation of afferents to this region. Future research will be necessary to fully understand circuit-level contributions to the development of novelty preference and social recognition of peers in order to potentially identify therapeutic targets for optimizing function in humans with social memory dysfunction due to neurodevelopmental disorders.

Supplementary Material

Refer to Web version on PubMed Central for supplementary material.

Acknowledgements:

The authors thank Samantha H. Wang for assistance with imaging and data collection and Alejandro J. Espinel for conducting the DeepLapCut huddling analysis. We thank Dr. Esteban Engel for generating both retroviruses and the retrograde AAV as well as Dr. María Llorens-Martín for providing protocols for fluorescent imaging of the GFP-Synaptophysin retrovirus.

Funding Information:

National Institutes of Health, Grant Number R01 MH118631-01

Data Availability Statement:

The data supporting this manuscript is available upon request

References

Angevine JB (1965). Time of neuron origin in the hippocampal region. An autoradiographic study in the mouse. Experimental Neurology, 11, 1–39. 10.1016/0014-4886(65)90121-4. [PubMed: 14272556]

Bailoo JD, Voelkl B, Varholick J, Novak J, Murphy E, Rosso M, Palme R, Würbel H (2020) Effects of weaning age and housing conditions on phenotypic differences in mice. Scientific Reports, 10, 11684. 10.1038/s41598-020-68549-3 [PubMed: 32669633]

Berger B, Esclapez M, Alvarez C, Meyer G and Catala M (2001). Human and monkey fetal brain development of the supramammillary-hippocampal projections: A system involved in the regulation of theta activity. Journal of Comparative Neurology, 429: 515–529. 10.1002/hipo.23296 [PubMed: 11135232]

Burnham D (1993). Visual recognition of mother by young infants: facilitation by speech. Perception, 22(10), 1133–1153. 10.1068/p221133 [PubMed: 8047405]

Carstens KE, Phillips ML, Pozzo-Miller L, Weinberg RJ, & Dudek SM (2016). Perineuronal nets suppress plasticity of excitatory synapses on CA2 pyramidal neurons. The Journal of Neuroscience, 36(23), 6312–6320. https://doi.org/10.1523/JNEUROSCI.0245-16.2016https://doi.org/10.1002/1096-9861(20010122)429:4<515::AID-CNE1>3.0.CO;2-2 [PubMed: 27277807]

Bilkei-Gorzo A, Mauer D, Michel K, & Zimmer A (2014). Dynorphins regulate the strength of social memory. Neuropharmacology, 77, 406–413. 10.1016/j.neuropharm.2013.10.023 [PubMed: 24184385]

Boehringer R, Polygalov D, Huang A, Middleton SJ, Robert V, Wintzer ME, Piskorowski RA, Chevaleyre V, & McHugh TJ (2017). Chronic loss of CA2 transmission leads to hippocampal hyperexcitability. Neuron, 94(3), 642–655.e9. 10.1016/j.neuron.2017.04.014 [PubMed: 28472661]

Briones BA, Pisano TJ, Pitcher MN, Haye AE, Diethorn EJ, Engel EA, Cameron HA, & Gould E (2021). Adult-born granule cell mossy fibers preferentially target parvalbumin-positive interneurons surrounded by perineuronal nets. Hippocampus, 31(4), 375–388. h [PubMed: 33432721]

Chen S, He L, Huang AJY, Boehringer R, Robert V, Wintzer ME, Polygalov D, Weitemier AZ, Tao Y, Gu M, Middleton SJ, Namiki K, Hama H, Therreau L, Chevaleyre V, Hioki H, Miyawaki A, Piskorowski RA, & McHugh TJ (2020). A hypothalamic novelty signal modulates hippocampal memory. Nature, 586(7828), 270–274. 10.1038/s41586-020-2771-1 [PubMed: 32999460]

Chiang MC, Huang A, Wintzer ME, Ohshima T, & McHugh TJ (2018). A role for CA3 in social recognition memory. Behavioural Brain Research, 354, 22–30. 10.1016/j.bbr.2018.01.019 [PubMed: 29355673]

Clemens AM, Wang H, & Brecht M (2020). The lateral septum mediates kinship behavior in the rat. Nature Communications, 11(1), 3161. 10.1038/s41467-020-16489-x

Cope EC, Waters RC, Diethorn EJ, Pagliai KA, Dias CG, Tsuda M, Cameron HA, & Gould E (2020). Adult-born neurons in the hippocampus are essential for social memory maintenance. ENeuro, 7(6), 1–12. 10.1523/ENEURO.0182-20.2020

Cui Z, Gerfen CR, & Young WS (2013). Hypothalamic and other connections with the dorsal ca2 area of the mouse hippocampus. The Journal of Comparative Neurology, 521(8), 1844–1866. 10.1002/cne.23263 [PubMed: 23172108]

Damon F, Quinn P, & Pascalis O (2021). When novelty prevails on familiarity: Visual biases for child versus infant faces in 3.5- to 12-month-olds. Journal of Experimental Child Psychology, 210. 10.1016/j.jecp.2021.105174

Domínguez S, Rey CC, Therreau L, Fanton A, Massotte D, Verret L, Piskorowski RA, & Chevaleyre V (2019). Maturation of PNN and ErbB4 signaling in area CA2 during adolescence underlies the emergence of pv interneuron plasticity and social memory. Cell Reports, 29(5), 1099–1112.e4. 10.1016/j.celrep.2019.09.044 [PubMed: 31665627]

Dudek SM, Alexander GM, & Farris S (2016). Rediscovering area CA2: Unique properties and functions. Nature Reviews Neuroscience, 17(2), 89–102. 10.1038/nrn.2015.22 [PubMed: 26806628]

Goursaud A-PS, Wallen K, & Bachevalier J (2014). Mother recognition and preference after neonatal amygdala lesions in rhesus macaques (Macaca mulatta) raised in a semi-naturalistic environment. Developmental Psychobiology, 56(8), 1723–1734. 10.1002/dev.21233 [PubMed: 25042548]

Guillory S, Baskett VZ, Grosman HE, McLaughlin CS, Isenstein EL, Wilkinson E, Weissman J, Britvan B, Trelles MP, Halpern DB, Buxbaum J, Siper PM, Wang AT, Kolevzon A, & Foss-Feig JH (2020). Social visual attentional engagement and memory in Phelan-McDermid syndrome and autism spectrum disorder: An eye-tracking study. Journal of Neurodevelopmental Disorders. 10.31234/osf.io/42d3f

Harshaw C, & Alberts JR (2012). Group and individual regulation of physiology and behavior: a behavioral, thermographic, and acoustic study of mouse development. Physiology & Behavior, 106(5), 670–682. 10.1016/j.physbeh.2012.05.002 [PubMed: 22580514]

Hitti FL, & Siegelbaum SA (2014). The hippocampal CA2 region is essential for social memory. Nature, 508(7494), 88–92. 10.1038/nature13028 [PubMed: 24572357]

Hofer M (1996). Multiple regulators of ultrasonic vocalization in the infant rat. Psychoneuroendocrinology, 21(2), 203–217. 10.1016/0306-4530(95)00042-9 [PubMed: 8774063]

Holsen LM, Dalton KM, Johnstone T, & Davidson RJ (2008). Prefrontal social cognition network dysfunction underlying face encoding and social anxiety in fragile X syndrome. NeuroImage, 43(3), 592–604. 10.1016/j.neuroimage.2008.08.009 [PubMed: 18778781]

Jones CE, & Monfils M-H (2016). Dominance status predicts social fear transmission in laboratory rats. Animal Cognition, 19(6), 1051–1069. 10.1007/s10071-016-1013-2 [PubMed: 27411940]

Kohara K, Pignatelli M, Rivest AJ, Jung H-Y, Kitamura T, Suh J, Frank D, Kajikawa K, Mise N, Obata Y, Wickersham IR, & Tonegawa S (2014). Cell type-specific genetic and optogenetic tools reveal novel hippocampal CA2 circuits. Nature Neuroscience, 17(2), 269–279. 10.1038/nn.3614 [PubMed: 24336151]

Kostan KM, & Snowdon CT (2002). Attachment and social preferences in cooperatively-reared cotton-top tamarins. American Journal of Primatology, 57(3), 131–139. 10.1002/ajp.10040 [PubMed: 12111679]

Laham B, Diethorn EJ, & Gould E (2021). Newborn mice form lasting CA2-dependent memories of their mothers. Cell Reports, 34(4). 10.1016/j.celrep.2020.108668

Leung C, Cao F, Nguyen R, Joshi K, Aqrabawi AJ, Xia S, Cortez MA, Snead OC, Kim JC, & Jia Z (2018). Activation of entorhinal cortical projections to the dentate gyrus underlies social memory retrieval. Cell Reports, 23(8), 2379–2391. 10.1016/j.celrep.2018.04.073 [PubMed: 29791849]

Lloréns-Martín M, Jurado-Arjona J, Avila J, & Hernández F (2015). Novel connection between newborn granule neurons and the hippocampal CA2 field. Experimental Neurology, 263, 285–292. 10.1016/j.expneurol.2014.10.021 [PubMed: 25446721]

Lopez-Rojas J, de Solis C, Leroy F, Kandel E, & Siegelbaum SA (2022). A direct lateral entorhinal cortex to hippocampal CA2 circuit conveys social information required for social memory. Neuron, 11(9), 1559–1572. 10.1016/j.neuron.2022.01.028

Martig AK, & Mizumori SJY (2011). Ventral tegmental area disruption selectively affects CA1/CA2 but not CA3 place fields during a differential reward working memory task. Hippocampus, 21(2), 172–184. 10.1002/hipo.20734 [PubMed: 20082295]

Martinez B, & Howe N (2013). Canadian early adolescents' self-disclosure to siblings and best friends. International Journal of Child, Youth and Family Studies, 4(2), 274. 10.18357/ijcyfs42201312212

Mathis A, Mamidanna P, Cury KM, Abe T, Murthy VN, Mathis MW, Bethge M (2018). DeepLabCut: markerless pose estimation of user-defined body parts with deep learning. Nature Neuroscience, 21, 1281–1289. 10.1038/s41593-018-0209-y [PubMed: 30127430]

McCann KE, Lustberg DJ, Shaughnessy EK, Carstens KE, Farris S, Alexander GM, Radzicki D, Zhao M, & Dudek SM (2021). Novel role for mineralocorticoid receptors in control of a neuronal phenotype. Molecular Psychiatry, 26(1), 350–364. 10.1038/s41380-019-0598-7 [PubMed: 31745235]

Meira T, Leroy F, Buss EW, Oliva A, Park J, & Siegelbaum SA (2018). A hippocampal circuit linking dorsal CA2 to ventral CA1 critical for social memory dynamics. Nature Communications, 9(1), 4163. 10.1038/s41467-018-06501-w

Montagrin A, Saiote C, & Schiller D (2018). The social hippocampus. Hippocampus, 28(9), 672–679. 10.1002/hipo.22797 [PubMed: 28843041]

Okuyama T (2018). Social memory engram in the hippocampus. Neuroscience Research, 129, 17–23. 10.1016/j.neures.2017.05.007 [PubMed: 28577978]

Oliva A, Fernández-Ruiz A, Leroy F, & Siegelbaum SA (2020). Hippocampal CA2 sharp-wave ripples reactivate and promote social memory. Nature, 587(7833), 264–269. 10.1038/s41586-020-2758-y [PubMed: 32968277]

Ophir AG (2017). Navigating monogamy: nonapeptide sensitivity in a memory neural circuit may shape social behavior and mating decisions. Frontiers in Neuroscience, 11. https://www.frontiersin.org/article/10.3389/fnins.2017.00397

Pascalis O, de Schonen S, Morton J, Deruelle C, & Fabre-Grenet M (1995). Mother's face recognition by neonates: A replication and an extension. Infant Behavior & Development, 18(1), 79–85. 10.1016/0163-6383(95)90009-8

Schaal B, Saxton T, Loos H, Soussignan R, & Durand K (2020). Olfaction scaffolds the developing human from neonate to adolescent and beyond. Philosophical Transactions of the Royal Society B: Biological Sciences. 10.1098/rstb.2019.0261

Sim S, Antolin S, Lin C-W, Lin Y-X, & Lois C (2013). Increased cell-intrinsic excitability induces synaptic changes in new neurons in the adult dentate gyrus that require Npas4. The Journal of Neuroscience, 33(18), 7928–7940. 10.1523/JNEUROSCI.1571-12.2013 [PubMed: 23637184]

Smith AS, Williams Avram SK, Cymerblit-Sabba A, Song J, & Young WS (2016). Targeted activation of the hippocampal CA2 area strongly enhances social memory. Molecular Psychiatry, 21(8), 1137–1144. 10.1038/mp.2015.189 [PubMed: 26728562]

Stanfield BB, Cowan WM. (1979) The development of the hippocampus and dentate gyrus in normal and reeler mice. J Comp Neurol.185(3):423–59. doi: 10.1002/cne.901850303. [PubMed: 86549]

Terranova ML, & Laviola G (1995). Individual differences in mouse behavioural development: effects of precocious weaning and ongoing sexual segregation. Animal behaviour, 50(5), 1261–1271. 10.1016/0003-3472(95)80042-5

Tibbetts EA, Pardo-Sanchez J, & Weise C (2022). The establishment and maintenance of dominance hierarchies. Philosophical Transactions of the Royal Society B: Biological Sciences, 377(1845), 20200450. 10.1098/rstb.2020.0450

van Praag H, Schinder AF, Christie BR, Toni N, Palmer TD, & Gage FH (2002). Functional neurogenesis in the adult hippocampus. Nature, 415(6875), 1030–1034. 10.1038/4151030a [PubMed: 11875571]

Wagatsuma A, Okuyama T, Sun C, Smith LM, Abe K, & Tonegawa S (2018). Locus coeruleus input to hippocampal CA3 drives single-trial learning of a novel context. Proceedings of the National Academy of Sciences, 115(2). 10.1073/pnas.1714082115

Williams TA, Porter MA, & Langdon R (2012). Viewing social scenes: A visual scan-path study comparing fragile X syndrome and Williams syndrome. Journal of Autism and Developmental Disorders, 43(8), 1880–1894. 10.1007/s10803-012-1737-z

Winslow JT, Hastings N, Carter CS, Harbaugh CR, & Insel TR (1993). A role for central vasopressin in pair bonding in monogamous prairie voles. Nature, 365(6446), 545–548. 10.1038/365545a0 [PubMed: 8413608]

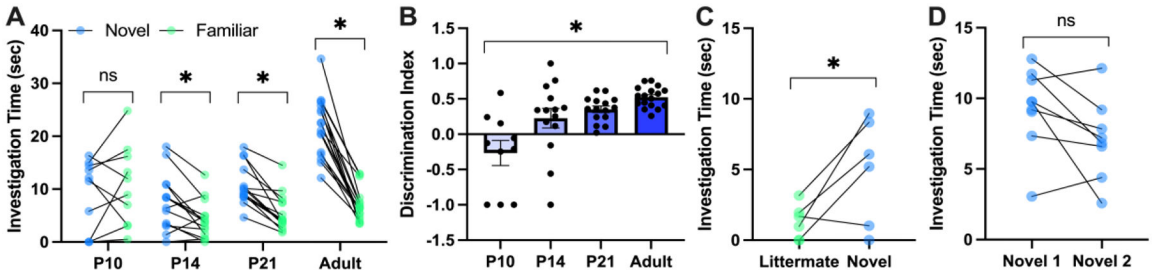

Figure 1.

Social preference for novel peers emerges at the end of the second postnatal week and increases with age. A) At P10, pups do not exhibit a significant difference in investigation time between novel and familiar recently encountered peers in the direct social interaction test. By contrast, P14, P21, and adult mice significantly prefer a novel mouse pup over a familiar one ($F_{(3, 52)} = 30.85$, $p < .0001$; P10: $p = .6763$, $N = 10$, P14: $p = .0479$, $N = 14$, P21: $p = .0004$, $N = 15$, Adult: $p < .0001$, $N = 17$). B) Discrimination indices ((novel minus familiar)/(novel plus familiar)) increase throughout development as preference for social novelty increases ($F_{(3, 52)} = 9.928$, $p < .0001$), and the P10 discrimination index is significantly different from all other ages (P10 vs. P14, $p = .0134$; P10 vs. P21, $p = .0009$; P10 vs. Adult, $p < .0001$). C-D) Findings in A and B from P14 mice are not due to fatigue between trials. C) P14 pups increase investigation time for a novel mouse in trial 2 compared to a familiar littermate in trial 1 ($t_5 = 2.672$, $p = .0442$, $N = 6$). D) P14 pups maintain relatively high levels of social investigation after consecutive presentations of novel pups ($t_8 = 0.9988$, $p = .3471$, $N = 9$). Related to Figure S1.

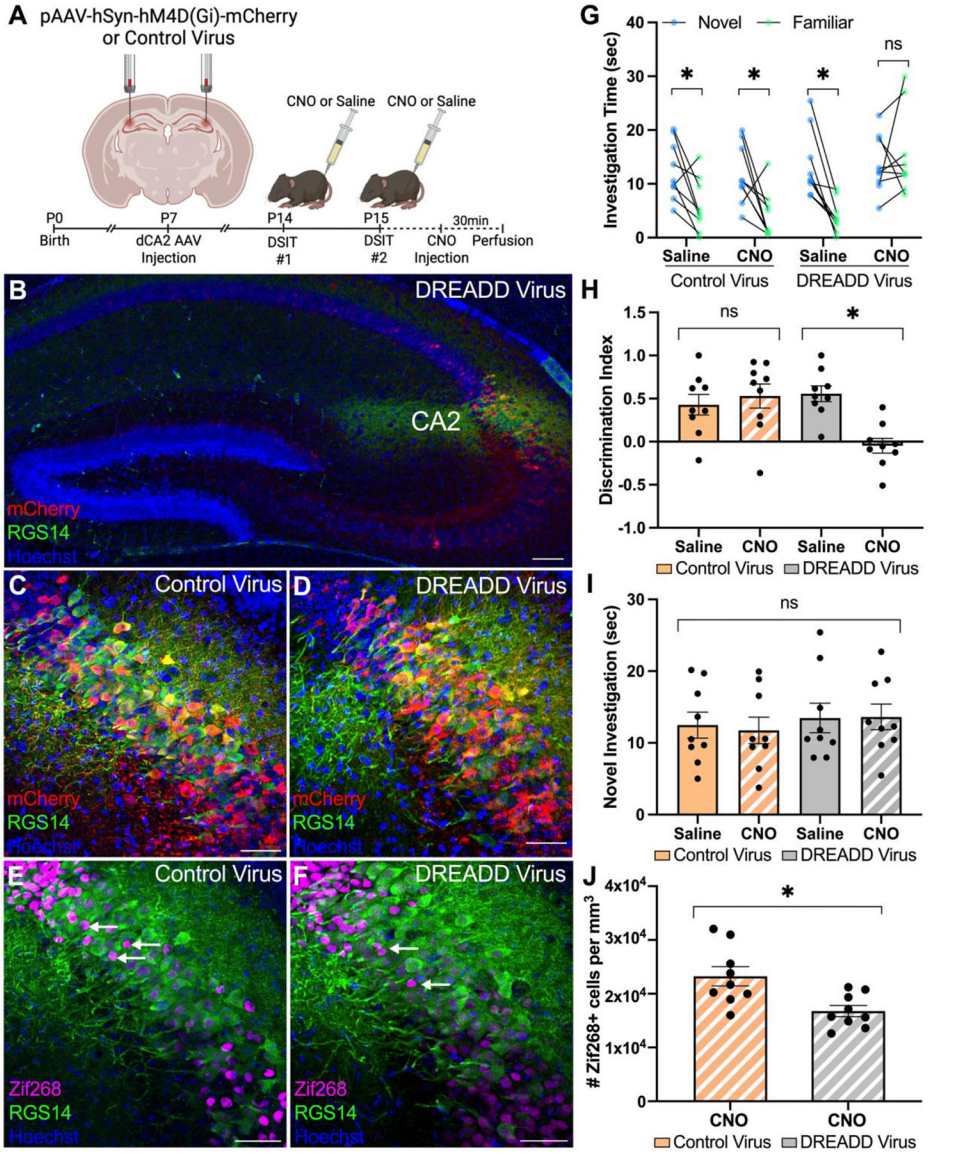

Figure 2.

Chemogenetic inhibition of CA2 neurons impairs social memory and preference for novel peers at P14/P15. A) Schematic of experimental design. B) Representative image of mCherry+ DREADD virus infection (red) in the RGS14+ CA2 (green) at 10x. C) Representative image of mCherry+ control virus infection in the RGS14+ CA2 at 30x. D) Representative image of mCherry+ DREADD virus infection in the RGS14+ CA2 at 30x. E) Representative image of Zif268 expression (magenta) in the RGS14+ CA2 (green) of a control virus animal. F) Representative image of Zif268 expression in the RGS14+ CA2 of a DREADD virus animal. G) Control virus animals ($N = 9$) administered both saline and CNO on consecutive days significantly prefer a novel peer in the direct social interaction test over a familiar peer (saline $p = .0428$, CNO $p = .0127$). DREADD virus animals ($N = 9$) administered saline significantly prefer a novel peer ($p = .0016$) but demonstrate impaired memory for a previously encountered peer when given CNO ($p = .9186$). H) Discrimination

indices between saline and CNO trials are equivalent in control virus animals ($p = .8533$), but in DREADD virus animals are significantly lower in the CNO trial compared to the saline trial ($p = .0154$). I) No interaction exists between time spent investigating the novel mouse in trial 1 and condition ($F_{(1, 16)} = 0.0617$, $p = .8069$). J) Zif268+ cell density is significantly lower in the CA2 of DREADD virus mice given CNO compared to control virus mice given CNO ($t_{16} = 3.115$, $p = .0067$). Scale bar = 50μm. Related to Figures S1–S3.

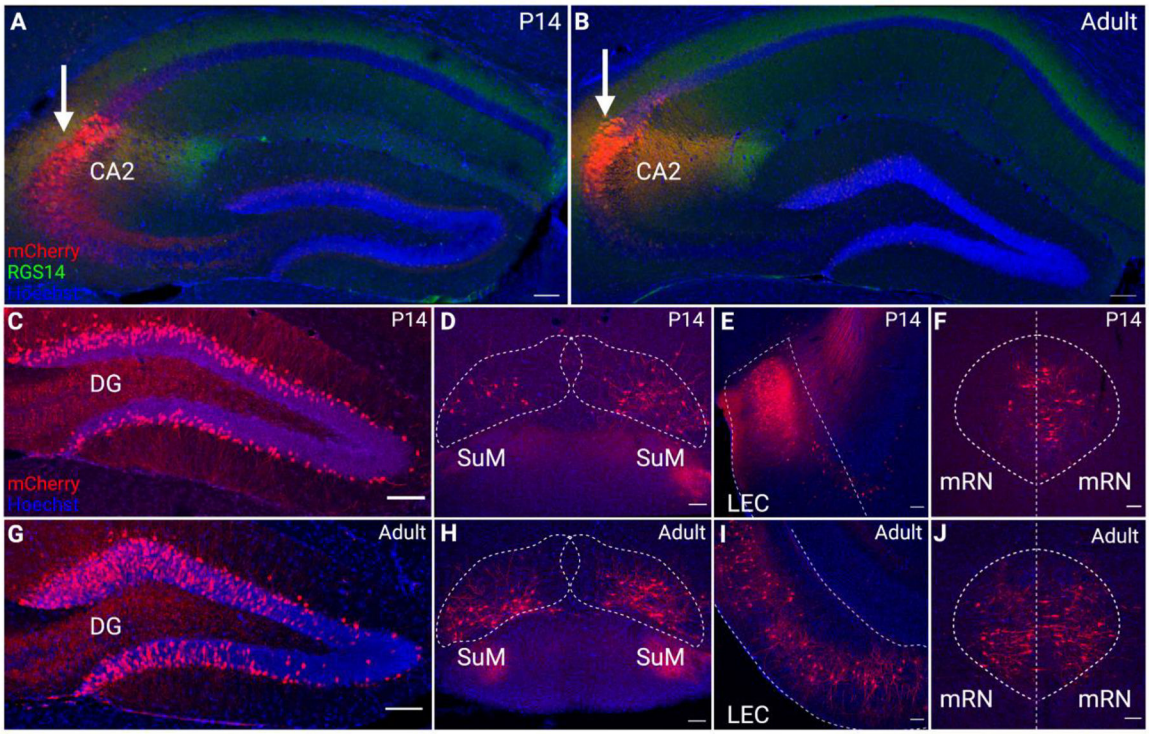

Figure 3.

Several CA2 afferent projections are present by P14 and appear comparable to those in the adult. A) Representative image of an mCherry+ retrograde AAV injection site (red) (white arrow) in the RGS14+ CA2 (green) of a P14-injected animal (−1.80mm AP). B) Representative image of mCherry+ retrograde AAV injection site (white arrow) in the RGS14+ CA2 of an adult-injected animal (−1.82mm AP). C-F) Retrograde labeling of CA2 afferents in a P14-injected animal perfused 2 WPI. C) mCherry+ dentate gyrus (DG) granule cells (−1.80mm AP). D) mCherry+ bilateral supramammillary nucleus (SuM) (−2.80mm AP). E) mCherry+ lateral entorhinal cortex (LEC) (−4.30mm AP). F) mCherry+ bilateral median raphe nucleus (mRN) (−4.30mm AP). G-J) Retrograde labeling of CA2 afferents in an adult-injected animal perfused 2 WPI. G) mCherry+ DG granule cells (−1.82mm AP). H) mCherry+ bilateral SuM (−3.00mm AP). I) mCherry+ LEC (−3.40mm AP). J) mCherry+ bilateral mRN (−4.00mm AP). All images are from coronal sections counterstained with Hoechst. Scale bar = 100μm.

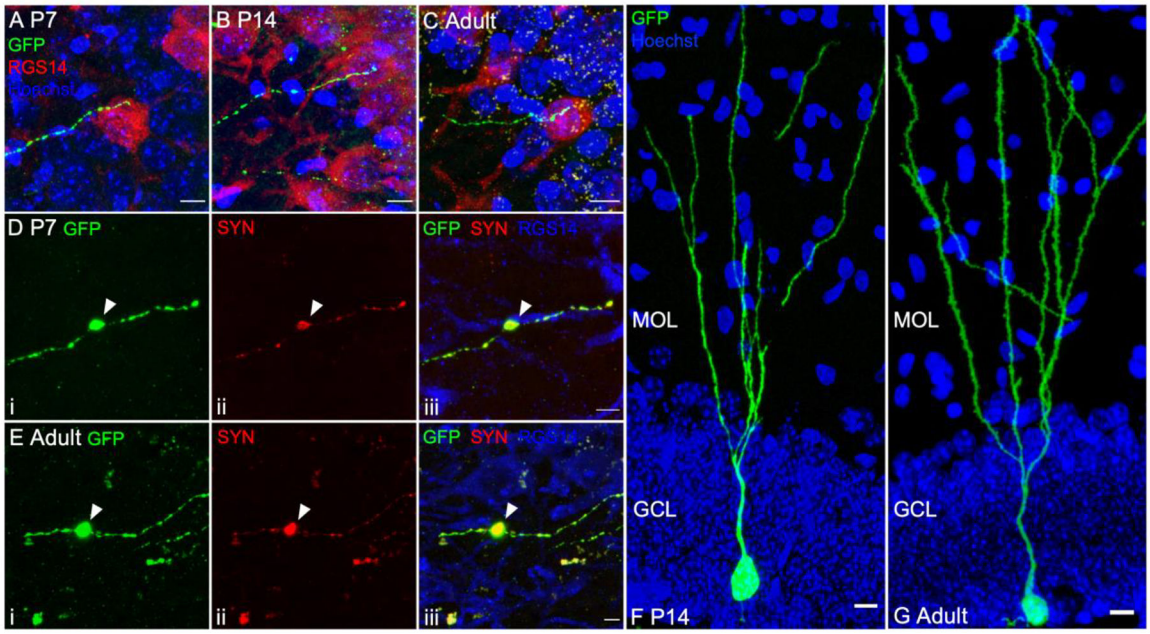

Figure 4.

Developmentally-born granule cells innervate the CA2 rapidly. A) P7-born GFP+ DG granule cells send mossy fibers to the RGS14+ CA2 by 2 WPI. B) P14-born granule cells send mossy fibers to the CA2 by 4 WPI. C) Adult-born granule cells send mossy fibers to the CA2 by 6 WPI. D) P7-born GFP+ (i) synaptophysin (SYN)+ (ii) mossy fibers innervate the CA2 (iii) at 2 WPI. E) Adult-born GFP+ (i) SYN+ (ii) mossy fibers innervate the CA2 (iii) at 6 WPI. F) GFP+ P14-born granule cell. G) GFP+ adult-born granule cell. Scale bar = 10μm.

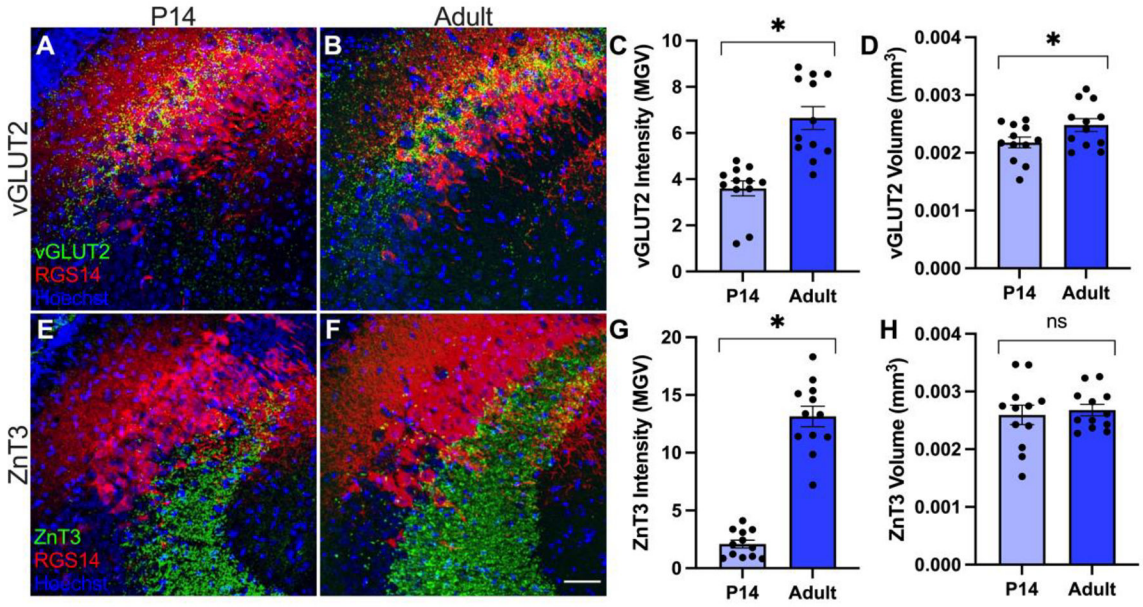

Figure 5.

Some CA2 afferents continue to mature between P14 and young adulthood. A-B) P14 (A) ($N = 12$) and adult (B) ($N = 12$) mice both show vGLUT2+ innervation (green) from the supramammillary nucleus to the RGS14+ CA2 (red). C) vGLUT2+ intensity increases in adulthood ($t_{22} = 5.142$, $p < .0001$). D) vGLUT2+ volume increases in adulthood ($t_{22} = 2.087$, $p = .0487$). E-F) P14 (E) and adult (F) mice both show ZnT3+ innervation (green) from the dentate gyrus to the RGS14+ CA2. G) ZnT3+ intensity increases in adulthood ($t_{22} = 11.71$, $p < .0001$). H) ZnT3+ volume remains the same between P14 and adulthood ($t_{22} = 0.4330$, $p = .6692$). Scale bar = 50μm.

Table 1.

Statistical Analyses

Data Set	Statistical Test	Main Effects	Post Hoc Comparisons
Figure 1A	Two-way ANOVA with repeated measures and Sidak's multiple comparisons (trial 1 vs. trial 2)	Trial $F_{(1, 52)} = 70.56$, $p < .0001$ Age $F_{(3, 52)} = 11.48$, $p < .0001$ Trial x Age $F_{(3, 52)} = 30.85$, $p < .0001$	P10: $p = .6763$ P14: $p = .0479$ P21: $p = .0004$ Adult: $p < .0001$
Figure 1B	One-way ANOVA with Sidak's multiple comparisons (discrimination index)	Age $F_{(3, 52)} = 9.928$, $p < .0001$	P10 vs. P14: $p = .0134$ P10 vs. P21: $p = .0009$ P10 vs. Adult: $p < .0001$ P14 vs. P21: $p = .9369$ P14 vs. Adult: $p = .1723$ P21 vs. Adult: $p = .7311$
Figure 1C	Paired t-test	$t_5 = 2.672$, $p = .0442$	n/a
Figure 1D	Paired t-test	$t_8 = 0.9988$, $p = .3471$	n/a
Figure 2G	Two-way ANOVA with repeated measures and Sidak's multiple comparisons (trial 1 vs. trial 2)	Trial $F_{(1, 32)} = 20.68$, $p < .0001$ Condition $F_{(3, 32)} = 4.781$, $p = .0073$ Trial x Condition $F_{(3, 32)} = 4.291$, $p = .0118$	Saline Control Virus: $p = .0428$ DREADD Virus: $p = .0016$ CNO Control Virus: $p = .0127$ DREADD Virus: $p = .9186$
Figure 2H	Two-way ANOVA with repeated measures and Šídák's multiple comparisons (saline index vs. CNO index)	Virus $F_{(1, 16)} = 9.881$, $p = 0063$ Treatment $F_{(1, 16)} = 3.211$, $p = .0921$ Virus x Treatment $F_{(1, 16)} = 6.315$, $p = .0231$	Control Virus Saline vs. CNO: $p = .8533$ DREADD Virus Saline vs. CNO: $p = .0154$
Figure 2I	Two-way ANOVA with repeated measures and Šídák's multiple comparisons (trial 1 saline vs. trial 1 CNO)	Virus $F_{(1, 16)} = 0.5425$, $p = .4720$ Treatment $F_{(1, 16)} = 0.0255$, $p = .8749$ Virus x Treatment $F_{(1, 16)} = 0.0617$, $p = .8069$	Control Virus Saline vs. CNO: $p = .9500$ DREADD Virus Saline vs. CNO: $p = .9976$
Figure 2J	Unpaired t-test	$t_{16} = 3.115$, $p = .0067$	n/a
Figure 5C	Unpaired t-test	$t_{22} = 5.142$, $p < .0001$	n/a
Figure 5D	Unpaired t-test	$t_{22} = 2.087$, $p = .0487$	n/a
Figure 5G	Unpaired t-test	$t_{22} = 11.71$, $p < .0001$	n/a
Figure 5H	Unpaired t-test	$t_{22} = 0.4330$, $p = .6692$	n/a
Figure S1B	One-way ANOVA with Šídák's multiple comparisons (huddling time)	Age $F_{(3, 52)} = 9.647$, $p < .0001$	P10 vs. P14: $p = .4056$ P10 vs. P21: $p = .0311$ P10 vs. Adult: $p < .0001$ P14 vs. P21: $p < .0001$ P14 vs. Adult: $p < .0001$ P21 vs. Adult: $p = .0966$
Figure S1C	Two-way ANOVA with repeated measures and Šídák's multiple comparisons (saline vs. CNO huddling time)	Virus $F_{(1, 16)} = 0.1832$, $p = .6744$ Treatment $F_{(1, 16)} = 3.131$, $p = .0959$ Virus x Treatment $F_{(1, 16)} = 0.04486$, $p = .8349$	Control Virus Saline vs. CNO: $p = .3281$ DREADD Virus Saline vs. CNO: $p = .4916$